Article

Cell Reports

Direct Gating of the TRPM2 Channel by cADPR via Specific Interactions with the ADPR Binding Pocket

Graphical Abstract

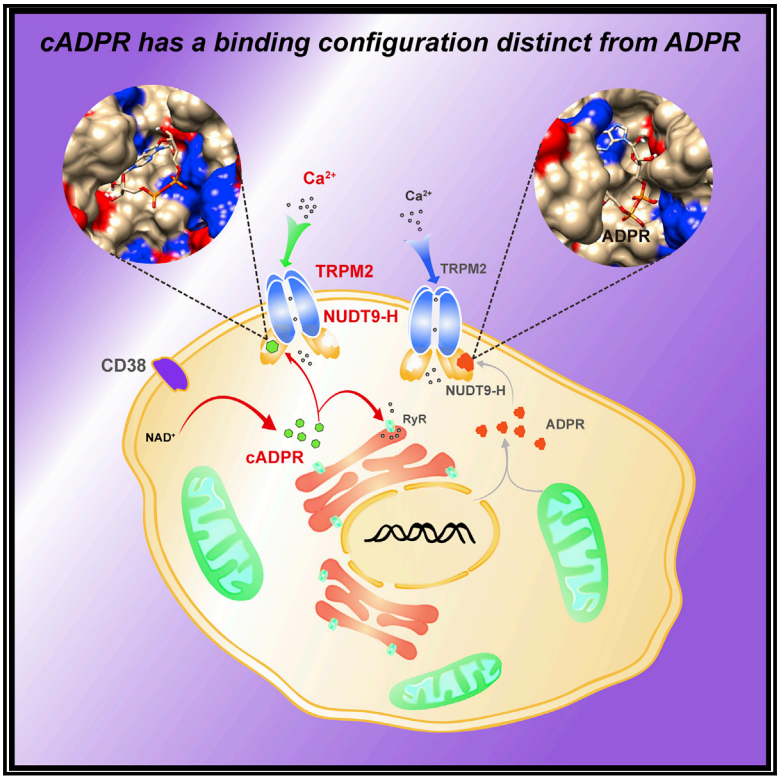

Highlights

- Purified cADPR directly activates the human TRPM2 channel (hTRPM2)
- Docking and simulation dynamics predict the binding pocket of cADPR in hTRPM2
- The binding affinity of cADPR with TRPM2 is less than that of ADPR by SPR assay
- The binding pattern of ADPR is different from that of cADPR with hTRPM2

Authors

Peilin Yu, Zhenming Liu, Xiafei Yu, ..., Liangren Zhang, Lihe Zhang, Wei Yang

Correspondence

yangwei@zju.edu.cn

In Brief

Yu et al. demonstrate that cADPR, which was thought to be an intracellular calcium messenger by modulating function of the ryanodine receptors (RyRs), also activates the TRPM2 channel. Their results suggest that cADPR regulates intracellular calcium release through multiple pathways.

Yu et al., 2019, Cell Reports 27, 3684–3695
June 18, 2019
https://doi.org/10.1016/j.celrep.2019.05.067

CellPress

OPEN ACCESS
CellPress

Cell Reports
Article

Direct Gating of the TRPM2 Channel by cADPR via Specific Interactions with the ADPR Binding Pocket

Peilin Yu,[1,2,10] Zhenming Liu,[3,10] Xiafei Yu,[1] Peiwu Ye,[1] Huan Liu,[1] Xiwen Xue,[3] Lixin Yang,[3] Zhongtang Li,[3] Yang Wu,[4] Cheng Fang,[4] Yong Juan Zhao,[4] Fan Yang,[1,9] Jian Hong Luo,[5] Lin-Hua Jiang,[6,7] Liangren Zhang,[3] Lihe Zhang,[3] and Wei Yang[1,8,11,*]

[1]Department of Biophysics, Institute of Neuroscience, NHC and CAMS Key Laboratory of Medical Neurobiology, Zhejiang University School of Medicine, Hangzhou 310058, P.R. China
[2]Department of Toxicology, School of Public Health, Zhejiang University, Hangzhou, Zhejiang 310058, P.R. China
[3]State Key Laboratory of Natural and Biomimetic Drugs, School of Pharmaceutical Sciences, Peking University, Beijing 100191, P.R. China
[4]Laboratory of Cytophysiology, State Key Laboratory of Chemical Oncogenomics, Key Laboratory of Chemical Genomics, Peking University Shenzhen Graduate School, Shenzhen, Guangdong 518055, P.R. China
[5]Department of Neurobiology, Institute of Neuroscience, NHC and CAMS Key Laboratory of Medical Neurobiology, Zhejiang University School of Medicine, Hangzhou, Zhejiang 310058, P.R. China
[6]School of Biomedical Sciences, Faculty of Biological Sciences, University of Leeds, Leeds LS2 9JT, UK
[7]Sino-UK Laboratory of Brain Function and Injury of Henan Province and Department of Physiology and Neurobiology, Xinxiang Medical University, Henan 453003, P.R. China
[8]Department of Neurosurgery, The First Affiliated Hospital, College of Medicine, Zhejiang University, Hangzhou, Zhejiang 310058, P.R. China
[9]Kidney Disease Center, The First Affiliated Hospital, College of Medicine, Zhejiang University, Hangzhou, Zhejiang 310058, P.R. China
[10]These authors contributed equally
[11]Lead Contact
*Correspondence: yangwei@zju.edu.cn
https://doi.org/10.1016/j.celrep.2019.05.067

SUMMARY

cADPR is a well-recognized signaling molecule by modulating the RyRs, but considerable debate exists regarding whether cADPR can bind to and gate the TRPM2 channel, which mediates oxidative stress signaling in diverse physiological and pathological processes. Here, we show that purified cADPR evoked TRPM2 channel currents in both whole-cell and cell-free single-channel recordings and specific binding of cADPR to the purified NUDT9-H domain of TRPM2 by surface plasmon resonance. Furthermore, by combining computational modeling with electrophysiological recordings, we show that the TRPM2 channels carrying point mutations at H1346, T1347, L1379, S1391, E1409, and L1484 possess distinct sensitivity profiles for ADPR and cADPR. These results clearly indicate cADPR is a *bona fide* activator at the TRPM2 channel and clearly delineate the structural basis for cADPR binding, which not only lead to a better understanding in the gating mechanism of TRPM2 channel but also shed light on a cADPR-induced RyRs-independent Ca^{2+} signaling mechanism.

INTRODUCTION

Nicotinamide adenine dinucleotide (NAD^+), a well-known enzyme cofactor, and its metabolites have emerged as key regulators of cellular and organismal homeostasis. Being a major component of both bioenergetic and signaling pathways, NAD^+ is ideally suited to regulate metabolism and major cellular events. Recent studies indicate that NAD^+ and its metabolites, including adenosine 5′-diphosphoribose (ADP-ribose), cyclic ADP-ribose (cADPR), and nicotinic acid adenine dinucleotide phosphate (NAADP) also function in cellular signaling by regulating many Ca^{2+}-permeable ion channels (Gasser et al., 2006; Koch-Nolte et al., 2008; Lee et al., 1995; Rusinko and Lee, 1989). For example, ADPR can trigger extracellular Ca^{2+} entry via activation of the plasma membrane cation channel transient receptor potential melastatin 2 (TRPM2) (Guse, 2015; Sumoza-Toledo and Penner, 2011); and NAADP activates the two-pore channels in the endolysosomes (Guse, 2015; Lee, 2012; Morgan and Galione, 2014; Patel et al., 2010).

cADPR is another important NAD^+ metabolite that has been recognized as a second messenger in a wide variety of cellular processes, including muscle contraction, release of insulin, secretion of neurotransmitters, and fertilization of oocytes (Bruzzone et al., 2007; Galione et al., 1991; Guse, 2004; Lee et al., 1989). It mediates Ca^{2+} signaling pathways by binding to FKBP12.6 and modulating the function of the ryanodine receptors (RyRs) (Bultynck et al., 2001; Noguchi et al., 1997; Tang et al., 2002). However, when RyRs were specifically blocked by a scorpion toxin, cADPR was still able to induce an increase in the intracellular Ca^{2+} concentrations in rabbit skeletal muscles, indicating that RyRs-independent mechanisms contribute to cADPR-induced Ca^{2+} responses (Morrissette et al., 1993). Moreover, cADPR can regulate Ca^{2+} influx through Ca^{2+}-permeable channels in neutrophils (Partida-Sánchez et al., 2001) and induce the Ca^{2+} spikes in T lymphocytes that were blocked by removal of extracellular Ca^{2+} or by perfusion with Zn^{2+} (Guse et al., 1997).

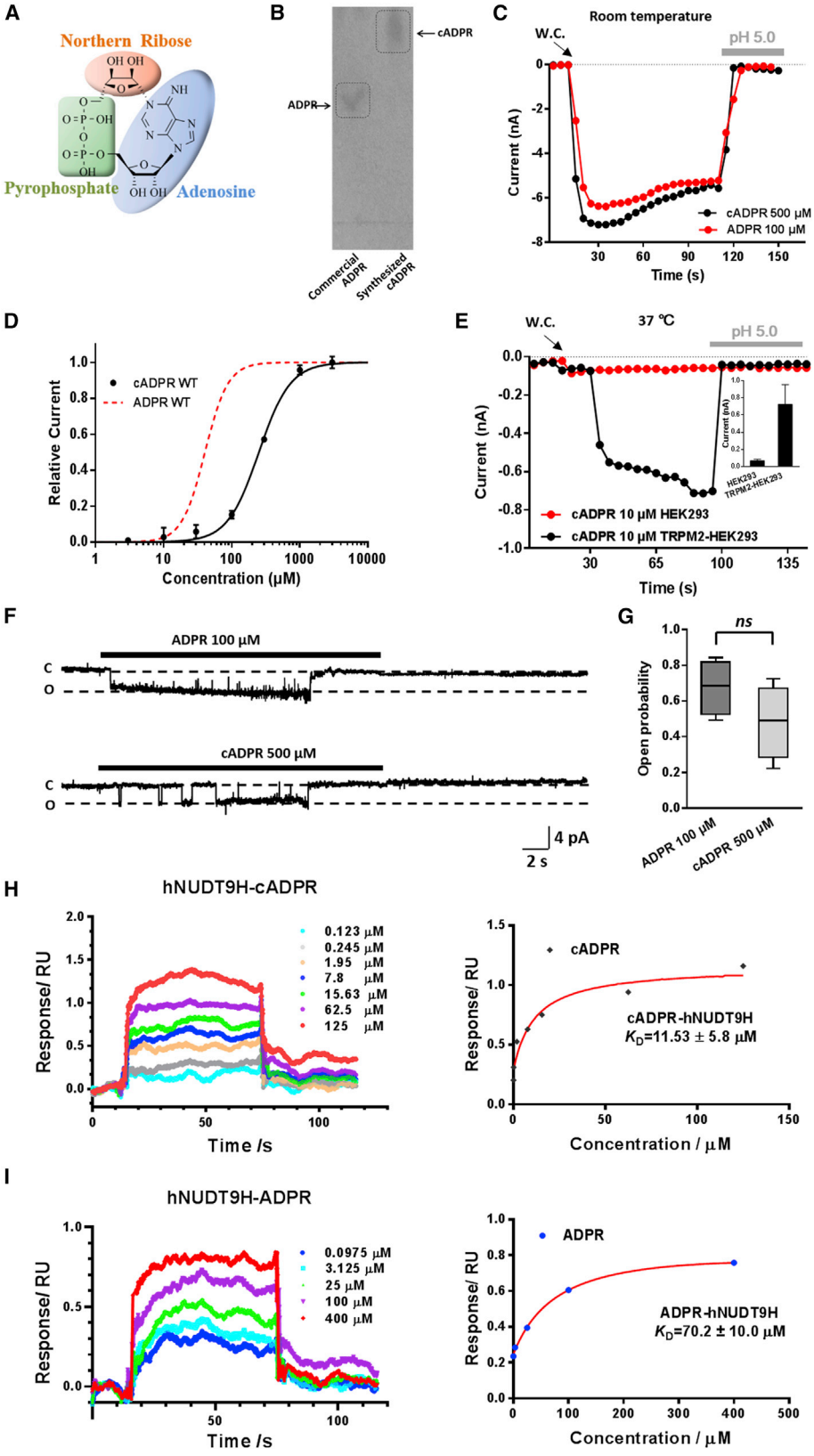

(legend on next page)

Therefore, in addition to Ca^{2+} release via RyRs, cADPR has been demonstrated to evoke extracellular Ca^{2+} entry, for which the TRPM2 channel has gained increasing attention.

The TRPM2 channel is a Ca^{2+}-permeable cation channel (Jiang et al., 2010) that functions as a sensor of oxidative stress resulting from an imbalanced redox state that leads to elevated reactive oxygen species (ROS) levels. Because increasing evidence supports a causative relationship between elevated ROS and a variety of disease conditions, such as diabetes, ischemia, neurodegeneration, and cancer (Chen et al., 2014; Kim et al., 2015; Manna et al., 2015; Ye et al., 2014; Jiang et al., 2018), to understand how the TRPM2 channel is gated by ligands is of great importance. The NUDT9 homology (NUDT9-H) domain in the C terminus of the TRPM2 channels is essential for binding of NAD^+ metabolites and thereby channel activation (Beck et al., 2006; Csanády and Törocsik, 2009; Hara et al., 2002; Kolisek et al., 2005; Lange et al., 2008; Perraud et al., 2001; Sano et al., 2001; Tóth and Csanády, 2012). Accumulating evidence indicates TRPM2 is a complex molecular machine crosslinked to several signaling pathways, uniquely linking the adenine nucleotide metabolic network to the intracellular redox status. So, it is critical to clarify the endogenous ligands from the NAD^+ metabolites that gate the TRPM2 channel.

Early studies reported that NAD^+ metabolites, including cADPR, activate the TRPM2 channel (Beck et al., 2006; Kolisek et al., 2005; Lange et al., 2008). However, recent studies have challenged that view and suggested that those earlier results might be compromised by ADPR contamination in the commercial cADPR (Tóth and Csanády, 2010; Tóth et al., 2015). Therefore, whether cADPR acts as a ligand for direct binding and activation of the TRPM2 channel is crucial to fully understanding the Ca^{2+} signaling mechanisms that it mediates.

Here, through a combination of surface plasmon resonance (SPR), whole-cell and single-channel patch-clamp recordings, cADPR-hydrolase activity assays, site-directed mutagenesis, and computational modeling, we investigated whether cADPR is a true ligand for the TRPM2 channel. Our results clearly demonstrate that cADPR is a *bona fide* activator of the TRPM2 channel. Furthermore, we have determined the key residues within the NUDT9-H domain that interact with cADPR and have revealed distinct modes of binding for cADPR and ADPR to the TRPM2 channel.

RESULTS

cADPR Directly Activates and Binds to the TRPM2 Channel

The structure of cADPR comprises three moieties: a northern ribose, a pyrophosphate, and an adenosine (Figure 1A). To exclude ADPR contamination in commercially available cADPR, as previously reported (Tóth and Csanády, 2010), we synthesized cADPR by previously established protocols (Lee and Aarhus, 1991). Thin-layer chromatography (TLC) analysis showed a single, distinct spot for synthesized cADPR, indicating no detectable ADPR contamination (Figure 1B). Like ADPR, with whole-cell recordings in HEK293 cells expressing the human TRPM2 channel, cADPR clearly induced large TRPM2 currents (Figure 1C) that were strongly inhibited by acidic pH 5.0 at room temperature, as shown in our previous studies (Yang et al., 2010). Although the amplitudes of the maximal currents induced by cADPR and ADPR were similar, the 50% effective concentration (EC_{50}) value for cADPR (251.1 ± 17.8 μM) was greater than that for ADPR (40.0 ± 4.5 μM) (Figure 1D), which is in agreement with previous reports (Beck et al., 2006; Kolisek et al., 2005). Similar to previous studies (Togashi et al., 2006), cADPR at 10 μM, which is close to its physiological concentration, also induced the TRPM2 channel currents at 37°C (Figure 1E). To exclude the possibility that cADPR activated the TRPM2 channel through intracellular signaling, we recorded in the inside-out configuration single-channel activity in cell-free-excised membrane patches and found that cADPR elicited single-channel opening in a similar fashion as that of ADPR (Figures 1F and 1G). Taken together, these results provide evidence to demonstrate that cADPR is an agonist that can directly gate the TRPM2 channel.

Then, to approach the question of whether cADPR binds to the ADPR-binding pocket formed by the NUDT9-H domain, we purified the NUDT9-H domain from *Rosetta* (DE3). To improve the poor solubility of the NUDT9-H protein in Tris solution, as previously reported (Iordanov et al., 2016; Tóth et al., 2014), *N*-dodecyl-β-D-maltoside (DDM) detergent was added to facilitate analysis of the binding affinities of this protein for cADPR, ADPR, and NAD^+ by the SPR technique (Figures S1A and S1B). We clearly observed that cADPR bound to the NUDT9-H protein in a concentration-dependent fashion, with a dissociation

Figure 1. cADPR Directly Activates and Binds to the TRPM2 Channel

(A) Chemical structure of cADPR.

(B) Analysis of synthesized cADPR using TLC with a C18 silica gel plate. The commercial ADPR was used as a control.

(C) Representative TRPM2 channel current traces induced by 500 μM cADPR in TRPM2-expressing HEK293 cells (black) at −80 mV at room temperature. W.C., whole-cell configuration.

(D) The concentration-current response relationship for cADPR and the wild-type (WT) TRPM2 channel. Data are expressed as means ± SEM from five independent preparations. All of the concentration-current response relationships for ADPR reported in our previous work are marked in this article as the red dotted line for comparison.

(E) Representative TRPM2 channel current traces induced by 10 μM cADPR in WT (red, n = 4 cells) and TRPM2-expressing (black, n = 5 cells) HEK293 cells at 37°C. The inset represents a summary of the currents.

(F) Representative single-channel recordings in TRPM2-expressing HEK293 cells exposed to 100 μM of ADPR (top) and 500 μM of cADPR (bottom).

(G) The open probability of single-TRPM2 channels activated by 100 μM of ADPR (n = 7 patches) and 500 μM of cADPR (n = 6 patches). Whiskers extend to the minimum and maximum values; horizontal bars represent medians. *ns*, no significant difference.

(H and I) SPR curves of cADPR (H) and ADPR (I) binding to NUDT9-H (left) and the representative binding curve (right). All binding affinity values are tested as described in the Method Details and determined according to three parallel experiments.

See also Figures S1 and S2.

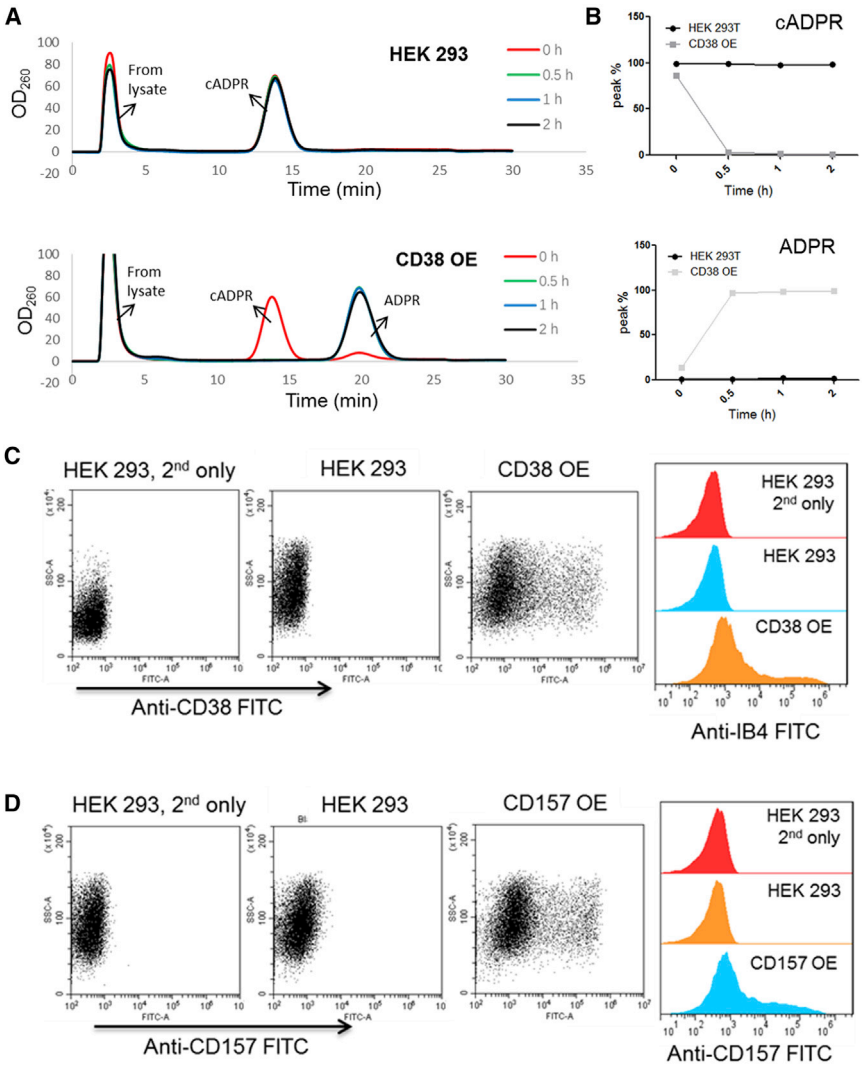

Figure 2. The Activity and Protein Expression of cADPR Hydrolases Are Not Detectable in HEK293 Cells

(A) The cADPR-hydrolase activity of the lysates from HEK293 cells (top) and CD38-overexpressing HEK293 cells (bottom).

(B) Quantitation of the relative contents of cADPR (top) and ADPR (bottom) at different time points in the reaction in (A).

(C and D) Immunostaining followed by flow cytometry to analyze the expression of CD38 (C) and CD157 (D) in HEK293 cells. Serving as positive controls, HEK293 cells were transfected with pcDNA3.1-CD38 (C) or pCMV3-CD157 (D) before analysis. The cells were briefly treated with 0.01% trypsin-EDTA for cell detachment and were stained with primary antibodies, anti-CD38 (C) or anti-CD157 (D). The dot plots (left panel) and histograms (right panel) of the flow cytometry analyses are shown.

constant (K_D) of 11.53 ± 5.8 μM (Figure 1H). As a positive control, our SPR results showed that ADPR bound to the NUDT9-H protein (K_D = 70.2 ± 10.0 μM) (Figure 1I). By contrast, NAD^+ did not bind to the NUDT9-H domain (Figure S1C), confirming the notion that NAD^+ does not act as a TRPM2 channel agonist (Yu et al., 2017).

cADPR Is Not Converted into ADPR in HEK293 Cells

Cluster of differentiation 38 (CD38) and CD157 belong to an evolutionarily conserved ADP-ribosyl cyclase gene family and have crucial roles in the reciprocal transformation of cADPR, NAADP, and ADPR (Graeff and Lee, 2013). To eliminate the possibility that cADPR was converted to ADPR by these enzymes and thereby activated the TRPM2 channel in HEK293 cells, commercial cADPR was first purified using high-performance liquid chromatography (HPLC) (Figure S2A). We found that cADPR was not contaminated by ADPR as identified by mass spectroscopy (MS) (Figures S2B and S2C). Then cADPR-hydrolase activity assays (Munshi et al., 2000) showed that lysates of HEK293 cells overexpressing CD38 hydrolyzed all cADPR into ADPR within 0.5 h, whereas lysates from wild-type (WT) or blank HEK293 cells did not decrease the cADPR peak even after 2 h, which was much longer than the duration of electrophysiological recordings (Figures 2A and 2B). These results indicate that WT HEK293 cells do not contain any detectable cADPR-hydrolase activity.

We further quantified the amount of cell-surface CD38 and CD157 in HEK293 cells by flow cytometry, followed by immunostaining with the specific antibodies. As shown in Figure 2C, the signal of anti-CD38 staining (middle dot plot, blue histogram) was basically identical to the negative control (2^{nd} antibody only, left dot plot, red histogram), although the cells transfected with CD38-expression plasmid showed significant anti-CD38 antibody staining (right dot plot, orange histogram). Similar results were obtained in WT and CD157-overexpressing HEK293 cells by anti-CD157 staining (Figure 2D). These results further demonstrate that HEK293 cells express neither CD38 nor CD157 or that the expression levels are below the detection by immunostaining, which excluded the possibility that cADPR indirectly activates the TRPM2 channel in HEK293 cells via enzymatic conversion to ADPR.

Molecular Docking and Molecular Dynamics (MD) Simulation Predict Binding of cADPR to the ADPR-Binding Pocket

Recent studies reported the structures of the sea anemone (*Nematostella vectensis* [nv]) TRPM2, zebrafish (*Danio rerio*) TRPM2, and human TRPM2 (Huang et al., 2018; Wang et al., 2018; Zhang et al., 2018). Although the structure of human TRPM2 in an ADPR-bound state has been resolved (Zhang

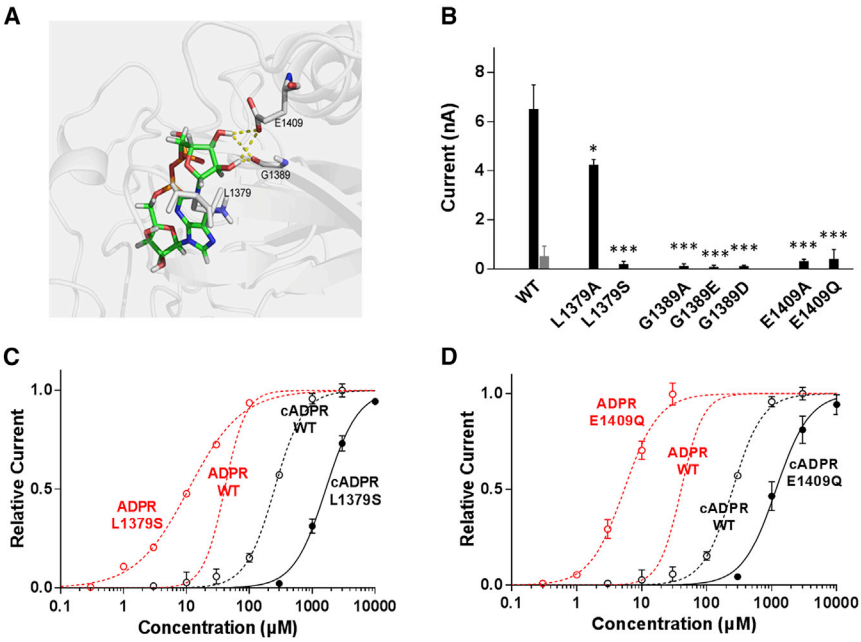

Figure 3. L1379, G1389, and E1409 in the NUDT9-H Domain Are Predicted to Interact with the Northern Ribose of cADPR

(A) Ribbon presentation of the northern ribose-binding pockets in the NUDT9-H domain (gray). The interactions are denoted with yellow dashed lines.

(B) Summary of the TRPM2 channel currents induced by EC_{10} (gray) and EC_{90} (black) concentrations of cADPR.

(C and D) Characterization of the cADPR concentration–current response relationship curves for WT (black dashed line) and mutants of L1379S (C) and E1409Q (D) of the TRPM2 channels (black continuous line).

All data are expressed as means ± SEM from five independent repeats. *p < 0.05, ***p < 0.001 versus WT.

et al., 2018), the binding pattern in this structure (6MIZ) is still unknown. We recently reported a subset of residues in the NUDT9-H domain to be critical in defining the ADPR-binding pocket at the TRPM2 channel (Yu et al., 2017). To further reveal the nature of cADPR binding to the NUDT9-H domain, similar molecular docking of cADPR, together with MD simulation, was conducted (Yu et al., 2017). The results predicted the same subset of residues interact with both cADPR and ADPR (Figure S3). More specifically, L1379, G1389, and E1409 interact with the northern ribose; H1346, T1347, S1391, and R1433 interact with the pyrophosphate group; and T1349, D1431, L1484, and H1488 interact with the adenosine base (Figure S3A). We further performed 15-ns equivalent simulations of the NUDT9-H with cADPR bound and examined each of the structurally identical binding sites with different ligands. The root-mean-square deviations (RMSDs) of the protein backbone atoms for the complex reached equilibrium after 9 ns at 4 Å for the cADPR-NUDT9-H complex (Figure S3B). We calculated, based on the frames from a 13- to 15-ns MD simulation trajectory, the total binding energy of cADPR binding (Table S1) and, moreover, the contributions of the 11 residues to the binding energy for cADPR, and assigned them into Van der Waals (VDW) force, electrostatic interaction, polar solvation, and non-polar solvation groupings (Tables S2). Although many residues exhibited similar energy contribution profiles for their interactions with cADPR and ADPR, the interaction patterns at several residues were predicted to be distinct between the two ligands, including H1346, T1347, and E1409. Such information supports the idea that these residues interact strongly with both ADPR and cADPR and that, as a ligand of the TRPM2 channel, cADPR has a binding configuration distinct from ADPR. So, we next performed a mutagenesis study to functionally analyze their types of interaction with, and involvement in, the TRPM2 channel activation by cADPR.

Mutations of Key Residues Interacting with the Northern Ribose Group Enlarge the Difference in the Sensitivity to ADPR and cADPR

L1379, G1389, and E1409 were predicted to interact with the northern ribose of cADPR (Figure 3A). L1379 was predicted to interact with this part via VDW forces (Table S2). L1379A mutation to shorten the side chain of Leu significantly reduced the currents induced by 500-μM cADPR (Figure 3B; p = 0.017). In addition, introduction of a polar group with L1379S mutation decreased the sensitivity to cADPR (Figure 3C). These results suggest that not only the VDW force but also a non-polar solvation interaction have important roles in the interactions with L1379.

For G1389, our MD simulation suggests occurrence of an electrostatic interaction between its carboxyl group and the hydroxyl group of the northern ribose ring of cADPR. We found none of G1389A, G1389E, and G1389D mutant channels was activated by cADPR at 500 μM (Figure 3B) or even at 3 mM (data not shown), which prevented us from constructing the concentration-response relationship curve. These results are similar to those for ADPR (Yu et al., 2017) and, overall, support the notion that the position of G1389 is critically required for cADPR-induced TRPM2 activation.

E1409 was predicted to have an electrostatic interaction between its hydroxyl oxygen atom and cADPR (Table S2), which is different from ADPR, which has a strong polar-solvation interaction with this residue (Yu et al., 2017). Consistent with this notion is that E1409Q mutation decreased the sensitivity to ADPR but increased the sensitivity to cADPR (Figure 3D; Table S3). These distinctive mutational effects likely result from exclusive impairment in the electrostatic interaction, indicating the importance of the electrostatic interaction between this residue and the terminal ribose of cADPR and supporting the hypothesis that cADPR have a distinct interaction configuration from ADPR.

Mutations of Key Residue Interacting with the Pyrophosphate Group Reverse the EC_{50} Values of ADPR and cADPR

Our MD simulation identified H1346, T1347, S1391, and R1433 as key residues that interact with the pyrophosphate group of

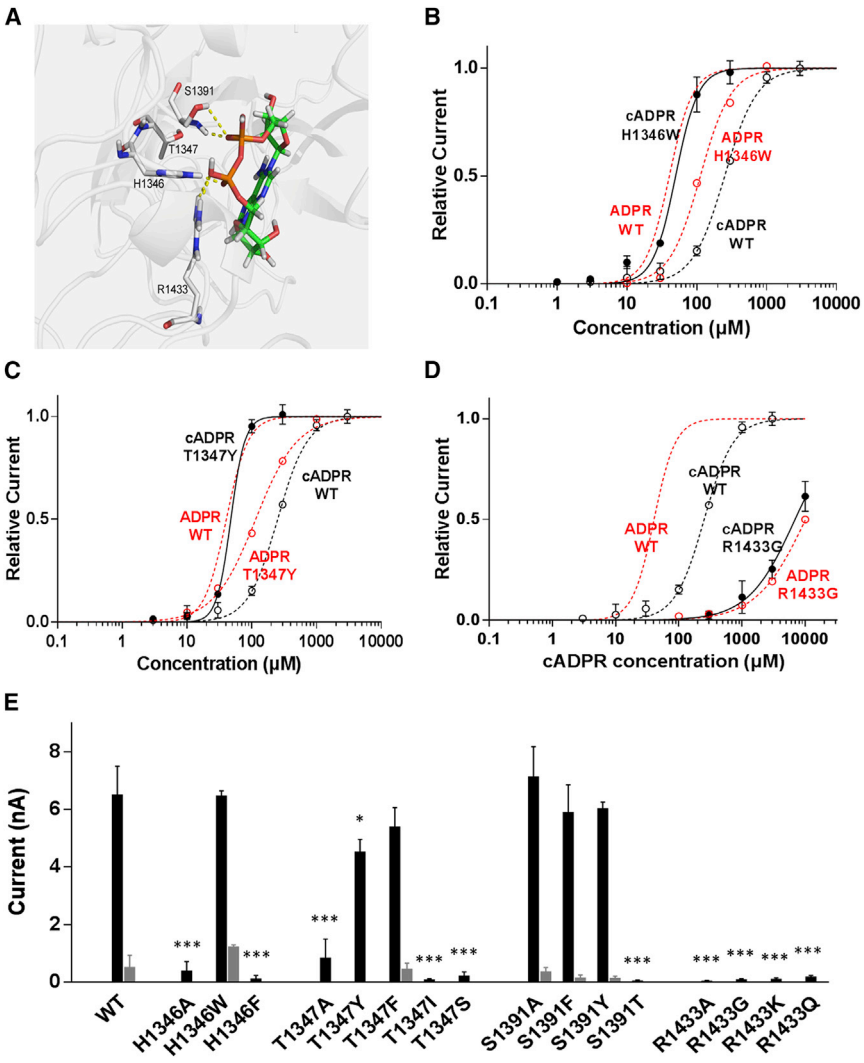

Figure 4. H1346, T1347, S1391, and R1433 of the NUDT9-H Domain Are Key Residues That Interact with the Pyrophosphate Group of cADPR

(A) Ribbon presentation of the pyrophosphate group binding pockets in the NUDT9-H domain (gray). The interactions are denoted with yellow dashed lines.

(B–D) Characterization of the cADPR concentration–current response relationship curves for WT (black dashed line) and mutants of H1346W (B), T1347Y (C), and R1433G (D) of the TRPM2 channels (black continuous line).

(E) Summary of the currents induced by EC_{10} (gray) and EC_{90} (black) concentrations of cADPR. Data are expressed as means ± SEM from five independent repeats. *p < 0.05, ***p < 0.001 versus WT.

cADPR (Figure 4A). For H1346, an electronic interaction was predicted (Table S2). Our mutagenesis results showed that neither the H1346A nor H1346F mutant responded to cADPR (Figure 4E), suggesting that the electronic interaction mediated by the imidazole ring of H1346 is critical for cADPR binding. In contrast, the H1346W mutant not only showed increased sensitivity to cADPR (Figure 4B; Table S3) but also changed its Hill slope (Table S3), supporting the idea that replacement with a benzene ring by this mutation facilitates the interactions between cADPR and this residue and the gating process. Of note, although H1346A and H1346F mutations caused similar change in the sensitivity to both cADPR and ADPR, the H1346W mutation resulted in opposite effects on channel activation by these two ligands, illustrating their difference in electrostatic interactions with H1346.

Another residue that had clearly different types of interactions in our previous MD simulation was T1347, which was predicted to have a polar-solvation interaction with cADPR (Table S2) but an electrostatic interaction with ADPR (Yu et al., 2017). Neither the mutants T1347A and T1347I, which would disrupt the polar-solvation interaction, nor the T1347S mutant, which would change the spatial location of polar-solvation interaction, was activated by cADPR (Figure 4E). The T1347F mutant, although it lost the polar-solvation interaction, still had an equivalent activation to the WT channel at both EC_{10} and EC_{90} concentrations of cADPR (Figure 4E) through an interaction with the introduced benzene ring of Phe. Interestingly, the T1347Y mutation, which slightly reduced the sensitivity to ADPR (Yu et al., 2017), strongly increased the sensitivity to cADPR (Figures 4C and 4E; p = 0.029; Table S3). This result may be due to a more prone position for the polar-solvation interaction between the hydroxyl group of this residue and cADPR when a benzene ring was introduced, also suggesting the different gating modes of cADPR and ADPR at this residue.

For S1391, although the MD simulation did not predict a substantial difference between cADPR and ADPR (Table S2), none of the mutations introduced into S1391 (S1391A, S1391F, and S1391Y) altered the sensitivity for cADPR (Figure 4E), whereas the S1391A mutant had a dramatically decreased EC_{50} for ADPR (Yu et al., 2017). In addition, the S1391T mutant, which introduced a methyl group and would change the direction of the hydroxyl group, was not activated by cADPR (Figure 4E), highlighting the importance of both presence and spatial position of the electrostatic interaction provided by the hydroxyl group of S1391.

A large contribution of polar-solvation interaction was predicted at R1433 (Table S2). Introduction of the R1433A mutation that disrupted the polar group resulted in a mutant channel with a much higher EC_{50} for cADPR (Figure 4E; Table S3); and the mutants with R1433K and R1433Q, which both changed the group that provided the polar-solvation interaction, were not activated by cADPR (Figure 4E), even at a high concentration of 3 mM (data

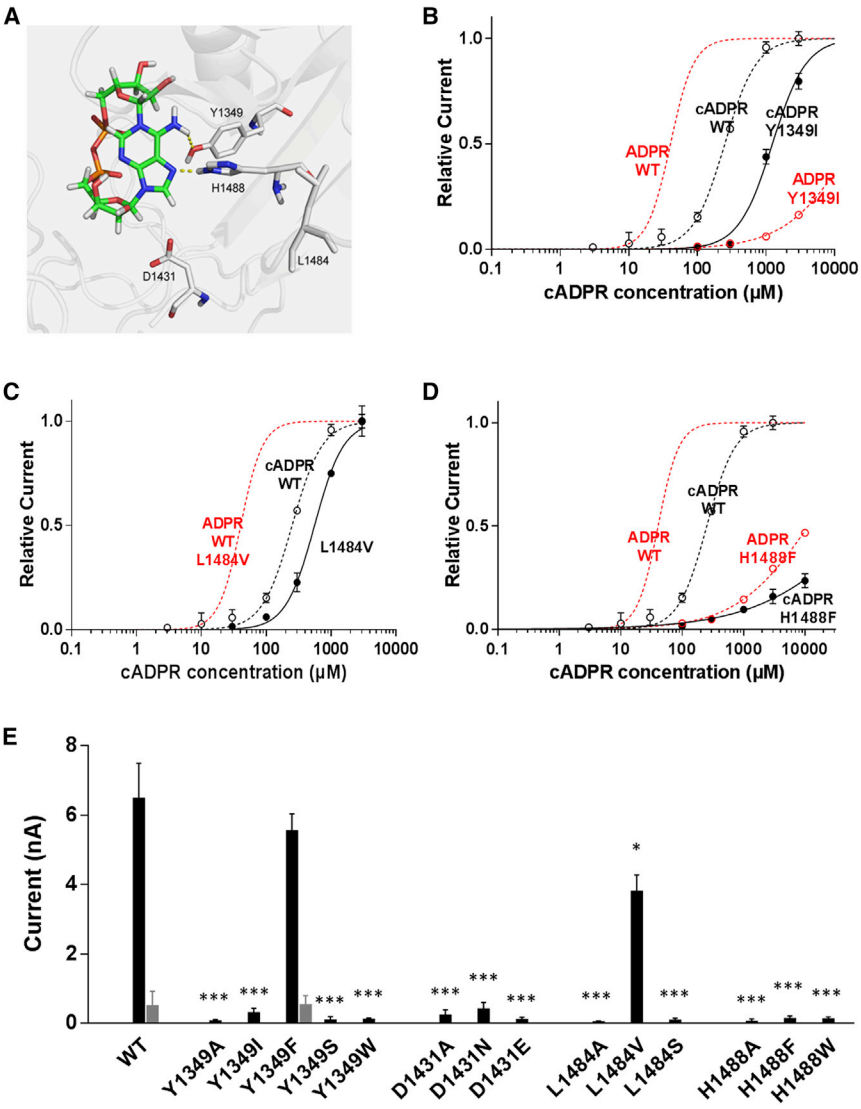

Figure 5. Y1349, D1431, L1484, and H1488 Residues in the NUDT9-H Domain Contribute to Interactions with the Adenosine Group of cADPR

(A) Ribbon presentation of the adenosine group binding pockets in the NUDT9-H domain (gray). The interactions are denoted with yellow dashed lines.

(B–D) Characterization of the cADPR concentration–current response relationship curves for WT (black dashed line) and indicated mutant TRPM2 channels (black continuous line).

(E) Summary of the currents induced by EC_{10} (gray) and EC_{90} (black) concentrations of cADPR. Data are expressed as means ± SEM from five independent repeats. *p < 0.05, ***p < 0.001 versus WT.

not shown). However, the R1433G mutant, with a shortened side chain length but still able to form a polar-solvation interaction, had a higher, but non-saturating, EC_{50} (Figure 4D; Table S3). These results demonstrate a strict requirement for the polar-solvation interaction at R1433.

Mutations of Key Residue Interacting with the Adenosine Group Impair the Channel Activation by ADPR and cADPR

The MD simulations predicted that Y1349, D1431, L1484, and H1488 residues contribute to interactions with the adenosine group of cADPR (Figure 5A). Similar contributions of polar-solvation interaction and VDW force were predicted for Y1349 (Table S2). In our functional assays, none of the mutants that changed the side chain length, no matter whether they preserved the polar group (Y1349A, Y1349S, and Y1349W), were activated by cADPR (Figure 5E). On the contrary, the mutants Y1349F and Y1349I, which lost the polar-solvation interaction but kept the VDW groups, were activated by cADPR with a similar (Y1349F) or higher (Y1349I) EC_{50} (Figures 5B and 5E; Table S3), suggesting a major contribution of VDW force from this residue.

Our simulation predicted a strong electrostatic interaction between D1431 and cADPR (Table S2). This was supported by the mutagenesis results showing that the D1431A mutant almost failed to respond to cADPR, whereas the D1431N mutant had a much higher EC_{50} for cADPR than that of the WT channel (Figure 5E; Table S3). Furthermore, the D1431E mutant with a longer side chain was also not activated by cADPR (Figure 5E). These results suggest that the electrostatic interaction of D1431 and its proper orientation are necessary for cADPR-induced TRPM2 channel activation.

In addition, a polar-solvation interaction was predicted for both L1484 and H1488 residues (Table S2). In the case of L1484, the L1484S mutant, in which a new polar group was introduced, was not activated by cADPR (Figure 5E). However, changing the spatial configuration of the side chain in the L1484V mutant resulted in a slight right-shift of the dose-response curve (Figure 5C and 5E; p = 0.013; Table S3), which indicates that the VDW force also has a role in the binding of cADPR to this residue. For H1488, the H1488F mutant, which lost the polar group, had a reduced sensitivity to cADPR (Figure 5D). However, although the polar-solvation interaction was preserved in the H1488W mutant, the steric hindrance caused by the benzene ring in this mutant made it unresponsive to cADPR (Figure 5E). These results provide evidence to support the idea that H1488 is critical for cADPR to activate the TRPM2 channel.

Our above results indicate ADPR and cADPR bind to the same pocket and, further, identify six residues that exhibit different interacting patterns between cADPR and ADPR. The E1409Q mutation resulted in the most distinct effect on the TRPM2 channel

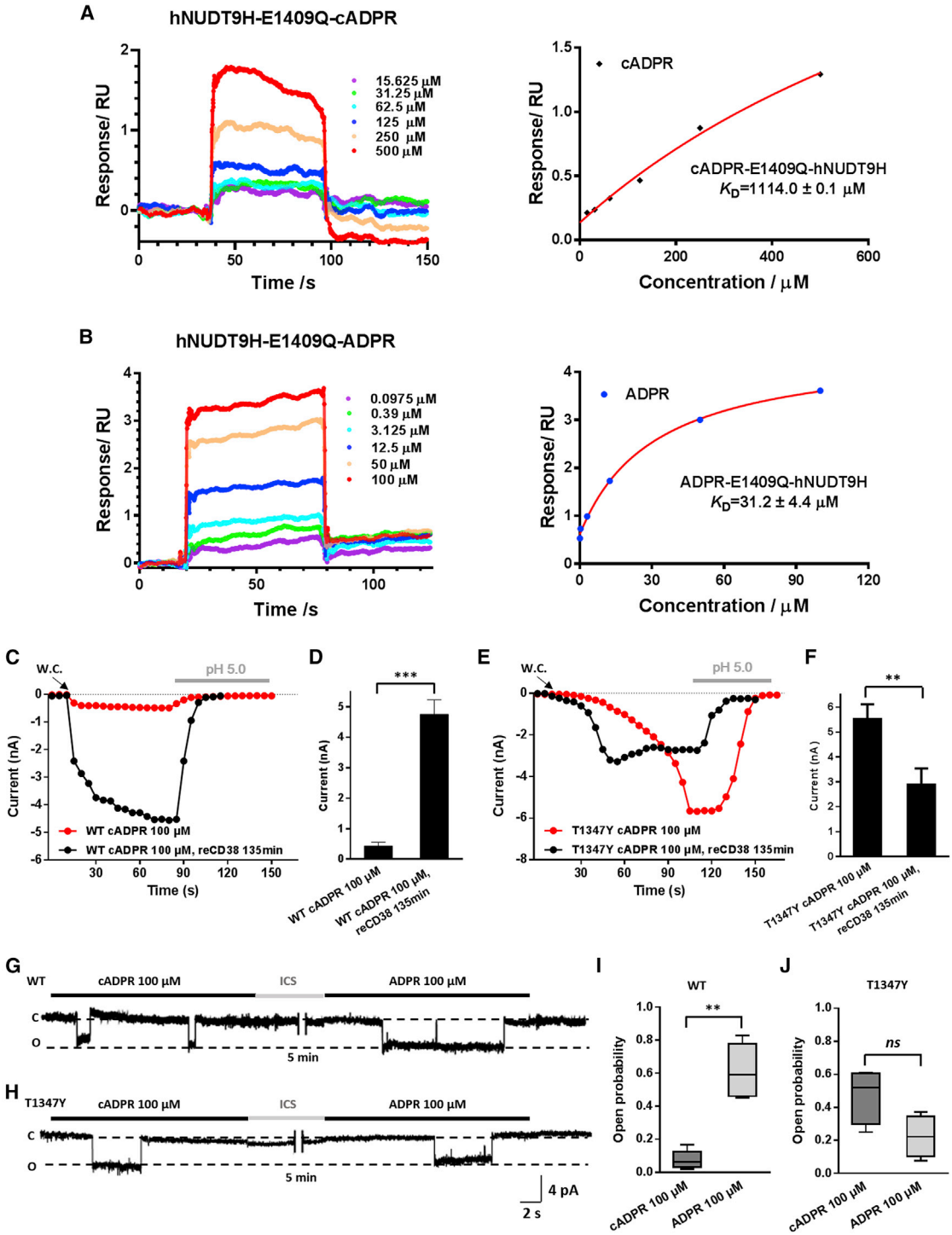

Figure 6. Residues That Exhibit Different Interacting Patterns between cADPR and ADPR

(A and B) The SPR curves of cADPR (A) and ADPR (B) binding to NUDT9-H-E1409Q (left) and the representative binding curve (right). All binding affinity values are determined according to three parallel experiments.

(C and E) Representative whole-cell TRPM2 channel current traces induced by 100 μM of cADPR without or with prior incubation with reCD38 in HEK293 cells expressing WT TRPM2 (C) and T1347Y mutant channel (E).

(D) Summary of the currents induced in (C) (n = 5 cells). Data are expressed as means ± SEM. **p < 0.01, ***p < 0.001.

(F) Summary of the currents in (E) (n = 5 cells). Data are expressed as means ± SEM. **p < 0.01, ***p < 0.001.

(legend continued on next page)

activation by ADPR and cADPR (Figure 3D). To further determine whether the E1409Q mutant changed the binding affinity of both ADPR and cADPR, we performed the SPR assay on the purified NUDT9-H E1409Q protein. The K_D value for cADPR was remarkably increased (1,114.0 ± 0.1 μM), whereas the binding affinity for ADPR was only slightly increased (K_D = 31.2 ± 4.4 μM) (Figures 6A and 6B), showing that this mutation resulted in a strong difference in altering the binding affinity for cADPR and ADPR, which is consistent with the electrophysiological results. Therefore, our data show that the binding affinity for cADPR was higher than ADPR, but the EC_{50} for ADPR in inducing TRPM2 activation was less than that for cADPR, which suggests that, upon binding, cADPR induces conformational changes to open the TRPM2 channel in a manner different from that of ADPR.

Besides E1409Q, T1347Y is another mutant that reversed the effects of ADPR and cADPR on TRPM2 activation. We further tested the effects of 100 μM of cADPR incubated without or with recombinant CD38 (reCD38) for 135 min on both WT TRPM2 and T1347Y mutant channels using whole-cell recordings. The sample composition after reCD38 incubation, analyzed by HPLC, showed that about half of the cADPR was converted to ADPR (Figure S4). Accordingly, 100 μM of cADPR after incubation with reCD38 significantly induced a larger WT TRPM2 channel current than did the sample without incubation (Figures 6C and 6D), but it induced a dramatically smaller current mediated by the mutant T1347Y channel than did the sample with incubation (Figures 6E and 6F). Furthermore, we compared the responses of WT and mutant T1347Y TRPM2 channels to 100 μM cADPR and ADPR in the same patch in single-channel recordings (Figures 6G and 6H). Consistent with the results in whole-cell recording (Figure 4C), the open probability of the WT channel induced by cADPR versus ADPR was the opposite of that of the mutant T1347Y channel at single-channel level (Figures 6I and 6J). Taken together, these results confirm the important role of T1347 in different binding modes of cADPR and ADPR in the NUDT9-H domain.

DISCUSSION

To identify the endogenous ligands for the TRPM2, it is critical to uncover the molecular basis for their binding to this channel. Here, we provide several lines of independent evidence using different techniques that consistently demonstrates that cADPR, an important messenger evoking Ca^{2+} signaling, can directly interact with, and open, the TRPM2 channel. In this study, we purified cADPR that showed no detectable trace of ADPR (Figures 1B and S2). With such purified cADPR, functional assays demonstrated that several mutants, including H1346W, L1347Y, L1379S, S1391A, E1409Q, and L1484V, had different sensitivity for ADPR versus cADPR. Single-channel recording and cADPR-hydrolase activity assays further excluded the possibility that cADPR activated the TRPM2 channel by converting to ADPR by ADP-ribosyl cyclases. Moreover, the results from SPR assays clearly indicate that cADPR binds to the NUDT9-H domain of TRPM2. Taken together, our results not only demonstrate that cADPR activates the TRPM2 channel (Kolisek et al., 2005; Togashi et al., 2006) but also establish that cADPR binds to the same pocket as ADPR does. A model of cADPR binding to this pocket in the NUDT9-H domain is presented in Figure 7, and the key residues we identified here are shown as green in Figure 7C. The different interactions at six residues between cADPR and ADPR further confirm that cADPR is, in fact, a ligand of the TRPM2 channel.

To activate the TRPM2 channel, a ligand needs to bind to the NUDT9-H domain and to induce conformational changes to open the channel pore. Generally, the EC_{50} value provides an indication of the capacity of these two distinctive processes in combination, whereas the SPR results mainly reflect only ligand binding. In our study, although the EC_{50} value of cADPR was much higher than that of ADPR for TRPM2 activation, the SPR results showed that the binding affinity of cADPR was higher than that of ADPR to the NUDT9-H domain, which may indicate the ability of cADPR to induce gating conformational changes is weaker than that of ADPR. Because cADPR has a glycosidic bond that locks its structure, ADPR is more flexible than cADPR is. Such structural flexibility in ADPR may facilitate induction of conformational changes and result in a lower EC_{50} value than that of cADPR. Moreover, our mutagenesis functional assays provided the supporting evidence: (1) mutation of Y1349, D1431, L1484, and H1488 residues, which interact with the adenosine group of cADPR and ADPR, markedly increased the EC_{50} values of both ADPR and cADPR, activating the TRPM2 channel, suggesting that the contributions of the adenosine group in ADPR and cADPR in the TRPM2 channel activation are similar; and (2) the residues, with the mutations exhibiting different interacting patterns between cADPR and ADPR, all interact with the terminal/northern ribose (L1379 and E1409) or the pyrophosphate group (H1346 and T1347) of ADPR and cADPR. These results suggest that the terminal/northern ribose and pyrophosphate moieties, which are important in determining the differential structural flexibility of cADPR and ADPR, might result in distinct sensitivity and gating properties of the TRPM2 channel.

On the other hand, despite several structures of TRPM2 being determined to show the overall architecture of this channel, these recent structural works have not revealed the ligand binding and gating mechanisms of the TRPM2 channel because (1) the structure of nv TRPM2 contains no intracellular domain, providing no information of ADPR binding (Zhang et al., 2018); (2) a recent study has resolved the structure of zebrafish TRPM2 by Cryo-electron microscopy (EM) where another ligand

(G and H) Representative single-channel recordings in cells expressing WT (G) and T1347Y mutant (H) TRPM2 channel in response to 100 μM of cADPR and 100 μM of ADPR on the same patch.

(I) Analysis of single-channel open probability for (G) (n = 5 patches). Whiskers extend to the minimum and maximum values; horizontal bars represent medians. **$p < 0.01$.

(J) Analysis of single-channel open probability for (n = 4 patches). Whiskers extend to the minimum and maximum values; horizontal bars represent medians. *ns*, no significant difference.

See also Figure S4.

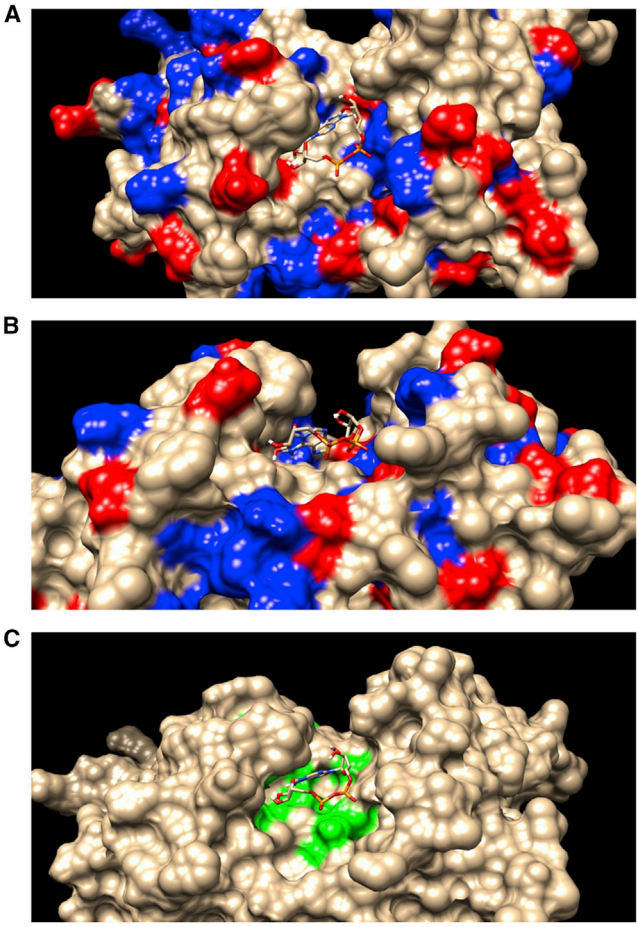

Figure 7. Structural Model of cADPR Binding to the NUDT9-H Domain Presented from Different Orientations

(A and B) Side (A) and top (B) view of cADPR binding in the NUDT9-H domain. The positively and negatively charged residues are, respectively, colored in blue and red.

(C) The whole view of the binding pocket of cADPR in the NUDT9-H domain. Critical residues for binding are labeled in green.

binding site exists in its N terminus (Huang et al., 2018); and (3) the structure of the human TRPM2 channel in the presence of ADPR has been resolved, but the binding pocket or key residues have not been defined (Wang et al., 2018). In addition, our recent study has shown the TRPM2 activation requires both intracellular calcium binding to its N terminus and ADPR acting on its C terminus (Luo et al., 2018). These studies all suggest the complexity of TRPM2 activation induced by the ligands. Because it is still unclear whether the N terminus of TRPM2 is involved in ADPR- and cADPR-induced TRPM2 activation, it will be interesting to determine the binding properties of these ligands to the N terminus and to uncover the relationship between the ligand binding sites on the N and C termini of TRPM2 for ligand-induced channel activation in the future. Meanwhile, to address these critical issues might be helpful in understanding why there are differential patterns between the binding affinities and EC_{50} values of ADPR versus cADPR.

cADPR has been widely recognized as a signaling molecule in species ranging from plants to mammals. To date, most studies have reported that cADPR increases the intracellular Ca^{2+} levels through activating the RyRs. A previous study also reported that cADPR at physiological conditions activated the TRPM2 channel (Togashi et al., 2006). Consistently, our data showed cADPR close to the physiological concentration was able to induce TRPM2 channel activation at body temperature, supporting the idea that TRPM2 is involved in cADPR-mediated intracellular Ca^{2+} signaling in many physiological and pathological processes. Although a recent study argues that cADPR is not an endogenous ligand of the TRPM2 channel (Tóth et al., 2015), our results provide clear evidence to support the earlier studies showing that cADPR is, indeed, a ligand that gates the TRPM2 channel. Our finding is also consistent with one of our earlier reports in which cIDPRE, a synthetic cADPR analog that is resistant to CD38 hydrolytic activity, activates the TRPM2 channels endogenously expressed in Jurkat T cells and exogenously expressed in HEK293 cells (Yu et al., 2012). In that study, we also reported that both RyR2 and RyR3 mediated the early phase of cADPR-induced Ca^{2+} responses, whereas the TRPM2 channel was responsible for the late and sustained phase in Jurkat T cells. These studies imply that both the RyRs and TRPM2 channels are responsible for cADPR-induced Ca^{2+} signaling. An attractive and reconciling hypothesis is that cADPR induces initial Ca^{2+} release via the RyRs and subsequently, in synergy with intracellular Ca^{2+}, evokes extracellular Ca^{2+} influx via the TRPM2 channel to generate a sustained Ca^{2+} signaling.

In summary, our results reveal TRPM2 as an identified target for cADPR, which directly activates this channel by binding to the same pocket as ADPR in the NUDT9-H domain but via distinct interactions. It will be very valuable to investigate the contribution of the TRPM2 channel in cADPR-mediated intracellular Ca^{2+} signaling in a variety of physiological or pathological processes.

STAR★METHODS

Detailed methods are provided in the online version of this paper and include the following:

- KEY RESOURCES TABLE
- LEAD CONTACT AND MATERIALS AVAILABILITY
- EXPERIMENTAL MODEL AND SUBJECT DETAILS
- METHOD DETAILS
  - High performance liquid chromatography (HPLC)
  - Electrophysiology
  - NUDT9-H protein purification
  - Surface plasmon resonance
  - cADPR hydrolase activity of HEK293 lysate
  - Immunostaining and flow cytometry
  - Docking and MD simulation
  - cADPR hydrolase incubation
- QUANTIFICATION AND STATISTICAL ANALYSIS

SUPPLEMENTAL INFORMATION

Supplemental Information can be found online at https://doi.org/10.1016/j.celrep.2019.05.067.

ACKNOWLEDGMENTS

We thank Prof. Jie Zheng for constructive discussion. This work was supported by grants from the Natural Science Foundation of China (81371302, 81571127, 31872796, 31471118, 21572010, 21772005, 31800990, 81673279, and 81573273); the National Basic Research Program of China (2014CB910300); National Major New Drugs Innovation and Development (2018ZX09711001-004-005); Zhejiang Provincial Natural Science Foundation (LR16H090001, LY19B020013); the 111 Project; the non-profit Central Research Institute Fund of Chinese Academy of Medical Sciences (2017PT31038, 2018PT31041); and University of Leeds-Zhejiang University Strategic Collaboration Partnership Programme.

AUTHOR CONTRIBUTIONS

W.Y., Z.L., and Liangren Zhang designed the research; P. Yu conducted the cADPR synthesis and purification, the patch-clamp recordings, and the data analysis; X.Y. and P. Ye contributed to the NUDT9-H protein purification; H.L. conducted part of the patch-clamp recordings; X.X. contributed to the ligand docking and MD simulation; L.Y. performed the SPR assay; Z.L. contributed to HPLC analysis; Y.W., C.F., and Y.J.Z. performed the cADPR-hydrolase activity assay; F.Y., J.H.L., L.-H.J., and Lihe Zhang participated in discussions, helped interpret the data, and revised the manuscript; and P. Yu and W.Y. prepared the paper.

DECLARATION OF INTERESTS

The authors declare no competing interests.

Received: September 26, 2018
Revised: February 5, 2019
Accepted: May 18, 2019
Published: June 18, 2019

REFERENCES

Beck, A., Kolisek, M., Bagley, L.A., Fleig, A., and Penner, R. (2006). Nicotinic acid adenine dinucleotide phosphate and cyclic ADP-ribose regulate TRPM2 channels in T lymphocytes. FASEB J. *20*, 962–964.

Bruzzone, S., Moreschi, I., Usai, C., Guida, L., Damonte, G., Salis, A., Scarfì, S., Millo, E., De Flora, A., and Zocchi, E. (2007). Abscisic acid is an endogenous cytokine in human granulocytes with cyclic ADP-ribose as second messenger. Proc. Natl. Acad. Sci. USA *104*, 5759–5764.

Bultynck, G., Rossi, D., Callewaert, G., Missiaen, L., Sorrentino, V., Parys, J.B., and De Smedt, H. (2001). The conserved sites for the FK506-binding proteins in ryanodine receptors and inositol 1,4,5-trisphosphate receptors are structurally and functionally different. J. Biol. Chem. *276*, 47715–47724.

Chen, S.J., Hoffman, N.E., Shanmughapriya, S., Bao, L., Keefer, K., Conrad, K., Merali, S., Takahashi, Y., Abraham, T., Hirschler-Laszkiewicz, I., et al. (2014). A splice variant of the human ion channel TRPM2 modulates neuroblastoma tumor growth through hypoxia-inducible factor (HIF)-1/2α. J. Biol. Chem. *289*, 36284–36302.

Colwill, K., Wells, C.D., Elder, K., Goudreault, M., Hersi, K., Kulkarni, S., Hardy, W.R., Pawson, T., and Morin, G.B. (2006). Modification of the Creator recombination system for proteomics applications—improved expression by addition of splice sites. BMC Biotechnol. *6*, 13.

Csanády, L., and Törocsik, B. (2009). Four Ca^{2+} ions activate TRPM2 channels by binding in deep crevices near the pore but intracellularly of the gate. J. Gen. Physiol. *133*, 189–203.

Fang, C., Li, T., Li, Y., Xu, G.J., Deng, Q.W., Chen, Y.J., Hou, Y.N., Lee, H.C., and Zhao, Y.J. (2018). CD38 produces nicotinic acid adenosine dinucleotide phosphate in the lysosome. J. Biol. Chem. *293*, 8151–8160.

Friesner, R.A., Banks, J.L., Murphy, R.B., Halgren, T.A., Klicic, J.J., Mainz, D.T., Repasky, M.P., Knoll, E.H., Shelley, M., Perry, J.K., et al. (2004). Glide: a new approach for rapid, accurate docking and scoring. 1. Method and assessment of docking accuracy. J. Med. Chem. *47*, 1739–1749.

Galione, A., Lee, H.C., and Busa, W.B. (1991). $Ca^{(2+)}$-induced Ca^{2+} release in sea urchin egg homogenates: modulation by cyclic ADP-ribose. Science *253*, 1143–1146.

Gasser, A., Bruhn, S., and Guse, A.H. (2006). Second messenger function of nicotinic acid adenine dinucleotide phosphate revealed by an improved enzymatic cycling assay. J. Biol. Chem. *281*, 16906–16913.

Graeff, R.M., and Lee, H.C. (2013). Determination of ADP-ribosyl cyclase activity, cyclic ADP-ribose, and nicotinic acid adenine dinucleotide phosphate in tissue extracts. Methods Mol. Biol. *1016*, 39–56.

Guse, A.H. (2004). Biochemistry, biology, and pharmacology of cyclic adenosine diphosphoribose (cADPR). Curr. Med. Chem. *11*, 847–855.

Guse, A.H. (2015). Calcium mobilizing second messengers derived from NAD. Biochim. Biophys. Acta *1854*, 1132–1137.

Guse, A.H., Berg, I., da Silva, C.P., Potter, B.V., and Mayr, G.W. (1997). Ca^{2+} entry induced by cyclic ADP-ribose in intact T-lymphocytes. J. Biol. Chem. *272*, 8546–8550.

Hara, Y., Wakamori, M., Ishii, M., Maeno, E., Nishida, M., Yoshida, T., Yamada, H., Shimizu, S., Mori, E., Kudoh, J., et al. (2002). LTRPC2 Ca^{2+}-permeable channel activated by changes in redox status confers susceptibility to cell death. Mol. Cell *9*, 163–173.

Huang, Y., Winkler, P.A., Sun, W., Lü, W., and Du, J. (2018). Architecture of the TRPM2 channel and its activation mechanism by ADP-ribose and calcium. Nature *562*, 145–149.

Iordanov, I., Mihályi, C., Tóth, B., and Csanády, L. (2016). The proposed channel-enzyme transient receptor potential melastatin 2 does not possess ADP ribose hydrolase activity. eLife *5*, e17600.

Jiang, L.H., Yang, W., Zou, J., and Beech, D.J. (2010). TRPM2 channel properties, functions and therapeutic potentials. Expert Opin. Ther. Targets *14*, 973–988.

Jiang, L.H., Li, X., Syed Mortadza, S.A., Lovatt, M., and Yang, W. (2018). The TRPM2 channel nexus from oxidative damage to Alzheimer's pathologies: An emerging novel intervention target for age-related dementia. Ageing Res. Rev. *47*, 67–79.

Kim, S.H., Smith, A.J., Tan, J., Shytle, R.D., and Giunta, B. (2015). MSM ameliorates HIV-1 Tat induced neuronal oxidative stress via rebalance of the glutathione cycle. Am. J. Transl. Res. *7*, 328–338.

Koch-Nolte, F., Kernstock, S., Mueller-Dieckmann, C., Weiss, M.S., and Haag, F. (2008). Mammalian ADP-ribosyltransferases and ADP-ribosylhydrolases. Front. Biosci. *13*, 6716–6729.

Kolisek, M., Beck, A., Fleig, A., and Penner, R. (2005). Cyclic ADP-ribose and hydrogen peroxide synergize with ADP-ribose in the activation of TRPM2 channels. Mol. Cell *18*, 61–69.

Lange, I., Penner, R., Fleig, A., and Beck, A. (2008). Synergistic regulation of endogenous TRPM2 channels by adenine dinucleotides in primary human neutrophils. Cell Calcium *44*, 604–615.

Lee, H.C. (2012). Cyclic ADP-ribose and nicotinic acid adenine dinucleotide phosphate (NAADP) as messengers for calcium mobilization. J. Biol. Chem. *287*, 31633–31640.

Lee, H.C., and Aarhus, R. (1991). ADP-ribosyl cyclase: an enzyme that cyclizes NAD^+ into a calcium-mobilizing metabolite. Cell Regul. *2*, 203–209.

Lee, H.C., Walseth, T.F., Bratt, G.T., Hayes, R.N., and Clapper, D.L. (1989). Structural determination of a cyclic metabolite of NAD^+ with intracellular Ca^{2+}-mobilizing activity. J. Biol. Chem. *264*, 1608–1615.

Lee, H.C., Aarhus, R., and Graeff, R.M. (1995). Sensitization of calcium-induced calcium release by cyclic ADP-ribose and calmodulin. J. Biol. Chem. *270*, 9060–9066.

Luo, Y., Yu, X., Ma, C., Luo, J., and Yang, W. (2018). Identification of a Novel EF-loop in the N-terminus of TRPM2 channel involved in calcium sensitivity. Front. Pharmacol. *9*, 581.

Manna, P.T., Munsey, T.S., Abuarab, N., Li, F., Asipu, A., Howell, G., Sedo, A., Yang, W., Naylor, J., Beech, D.J., et al. (2015). TRPM2-mediated intracellular Zn2+ release triggers pancreatic β-cell death. Biochem. J. *466*, 537–546.

Morgan, A.J., and Galione, A. (2014). Two-pore channels (TPCs): current controversies. BioEssays *36*, 173–183.

Morrissette, J., Heisermann, G., Cleary, J., Ruoho, A., and Coronado, R. (1993). Cyclic ADP-ribose induced Ca^{2+} release in rabbit skeletal muscle sarcoplasmic reticulum. FEBS Lett. *330*, 270–274.

Munshi, C., Aarhus, R., Graeff, R., Walseth, T.F., Levitt, D., and Lee, H.C. (2000). Identification of the enzymatic active site of CD38 by site-directed mutagenesis. J. Biol. Chem. *275*, 21566–21571.

Noguchi, N., Takasawa, S., Nata, K., Tohgo, A., Kato, I., Ikehata, F., Yonekura, H., and Okamoto, H. (1997). Cyclic ADP-ribose binds to FK506-binding protein 12.6 to release Ca^{2+} from islet microsomes. J. Biol. Chem. *272*, 3133–3136.

Partida-Sánchez, S., Cockayne, D.A., Monard, S., Jacobson, E.L., Oppenheimer, N., Garvy, B., Kusser, K., Goodrich, S., Howard, M., Harmsen, A., et al. (2001). Cyclic ADP-ribose production by CD38 regulates intracellular calcium release, extracellular calcium influx and chemotaxis in neutrophils and is required for bacterial clearance in vivo. Nat. Med. *7*, 1209–1216.

Patel, S., Marchant, J.S., and Brailoiu, E. (2010). Two-pore channels: regulation by NAADP and customized roles in triggering calcium signals. Cell Calcium *47*, 480–490.

Perraud, A.L., Fleig, A., Dunn, C.A., Bagley, L.A., Launay, P., Schmitz, C., Stokes, A.J., Zhu, Q., Bessman, M.J., Penner, R., et al. (2001). ADP-ribose gating of the calcium-permeable LTRPC2 channel revealed by Nudix motif homology. Nature *411*, 595–599.

Rusinko, N., and Lee, H.C. (1989). Widespread occurrence in animal tissues of an enzyme catalyzing the conversion of NAD^+ into a cyclic metabolite with intracellular Ca^{2+}-mobilizing activity. J. Biol. Chem. *264*, 11725–11731.

Sano, Y., Inamura, K., Miyake, A., Mochizuki, S., Yokoi, H., Matsushime, H., and Furuichi, K. (2001). Immunocyte Ca^{2+} influx system mediated by LTRPC2. Science *293*, 1327–1330.

Sumoza-Toledo, A., and Penner, R. (2011). TRPM2: a multifunctional ion channel for calcium signalling. J. Physiol. *589*, 1515–1525.

Tang, W.X., Chen, Y.F., Zou, A.P., Campbell, W.B., and Li, P.L. (2002). Role of FKBP12.6 in cADPR-induced activation of reconstituted ryanodine receptors from arterial smooth muscle. Am. J. Physiol. Heart Circ. Physiol. *282*, H1304–H1310.

Togashi, K., Hara, Y., Tominaga, T., Higashi, T., Konishi, Y., Mori, Y., and Tominaga, M. (2006). TRPM2 activation by cyclic ADP-ribose at body temperature is involved in insulin secretion. EMBO J. *25*, 1804–1815.

Tóth, B., and Csanády, L. (2010). Identification of direct and indirect effectors of the transient receptor potential melastatin 2 (TRPM2) cation channel. J. Biol. Chem. *285*, 30091–30102.

Tóth, B., and Csanády, L. (2012). Pore collapse underlies irreversible inactivation of TRPM2 cation channel currents. Proc. Natl. Acad. Sci. USA *109*, 13440–13445.

Tóth, B., Iordanov, I., and Csanády, L. (2014). Putative chanzyme activity of TRPM2 cation channel is unrelated to pore gating. Proc. Natl. Acad. Sci. USA *111*, 16949–16954.

Tóth, B., Iordanov, I., and Csanády, L. (2015). Ruling out pyridine dinucleotides as true TRPM2 channel activators reveals novel direct agonist ADP-ribose-2′-phosphate. J. Gen. Physiol. *145*, 419–430.

Wang, L., Fu, T.M., Zhou, Y., Xia, S., Greka, A., and Wu, H. (2018). Structures and gating mechanism of human TRPM2. Science *362*, 6421.

Yang, W., Zou, J., Xia, R., Vaal, M.L., Seymour, V.A., Luo, J., Beech, D.J., and Jiang, L.H. (2010). State-dependent inhibition of TRPM2 channel by acidic pH. J. Biol. Chem. *285*, 30411–30418.

Ye, M., Yang, W., Ainscough, J.F., Hu, X.P., Li, X., Sedo, A., Zhang, X.H., Zhang, X., Chen, Z., Li, X.M., et al. (2014). TRPM2 channel deficiency prevents delayed cytosolic Zn^{2+} accumulation and CA1 pyramidal neuronal death after transient global ischemia. Cell Death Dis. *5*, e1541.

Yu, P., Wang, Q., Zhang, L.H., Lee, H.C., Zhang, L., and Yue, J. (2012). A cell permeable NPE caged ADP-ribose for studying TRPM2. PLoS ONE *7*, e51028.

Yu, P., Xue, X., Zhang, J., Hu, X., Wu, Y., Jiang, L.H., Jin, H., Luo, J., Zhang, L., Liu, Z., and Yang, W. (2017). Identification of the ADPR binding pocket in the NUDT9 homology domain of TRPM2. J. Gen. Physiol. *149*, 219–235.

Zhang, Z., Tóth, B., Szollosi, A., Chen, J., and Csanády, L. (2018). Structure of a TRPM2 channel in complex with Ca^{2+} explains unique gating regulation. eLife *7*, e36409.

STAR★METHODS

KEY RESOURCES TABLE

REAGENT or RESOURCE	SOURCE	IDENTIFIER
Antibodies		
Rabbit polyclonal anti-CD38	homemade	N/A
Anti-CD157	Gifted by Fabio Malavasi, University of Torino Medical School	N/A
Anti-IB4	Gifted by Fabio Malavasi, University of Torino Medical School	N/A
FITC-conjugated anti-CD38	Homemade	N/A
FITC-conjugated anti-CD157	Homemade	N/A
TRPM2 Polyclonal Antibody	Invitrogen	OST00030W; AB_2208499
Bacterial and Virus Strains		
RosettagamiB(DE3) Competent Cells	TransGen Biotech	CD801
Chemicals, Peptides, and Recombinant Proteins		
cADPR	Homemade	N/A
cADPR	Sigma-Aldrich	C7344
ADPR	Sigma-Aldrich	A0752
NAD^+	Sigma-Aldrich	N7004
DMEM	GIBCO	11995-065
Penicillin-Streptomycin	GIBCO	15140-122
HBSS	GIBCO	14025-092
0.25% Trypsin-EDTA	GIBCO	25200-072
FBS Premium	PAN	ST30-3302
CH_3CN	Sigma-Aldrich	34851
Trifluoroacetic acid	Sigma-Aldrich	302031
HEPES	Sigma-Aldrich	H3375
Potassium D-gluconate	Aladdin	P108903
EGTA	Biosharp	Amresco 0732
glucose	Sigma-Aldrich	G8270
PBS	Homemade	N/A
Fetal Bovine Serum	GIBCO	10091148
Trypsin-EDTA (0.25%)	GIBCO	25200072
DMEM, powder, high glucose	GIBCO	12100061
Penicillin-Streptomycin (5,000 U/mL)	GIBCO	15070063
Trifluoroacetic acid	Sigma-Aldrich	302031
Bovine Serum Albumin	Sigma-Aldrich	A1933
Lipofectamine 2000 Transfection Reagent	Invitrogen	11668019
PBS-P+ buffer, 10X	GE Healthcare	Lot#244311
Protease Inhibitor Cocktail, mini-Tablet	MCE	HY-K0011
Glutathione reduced	BBI	A600229
LB Broth Powder, Miller	BBI	A507002
IPTG	Invitrogen	15529019
gluthathione Sepharose 4B resin	GE Healthcare	17-0757-01
thrombin protease	GIBCO	RP-43100
N-dodecyl-β-d-maltopyranoside	Anatrace	16494

(*Continued on next page*)

Continued

REAGENT or RESOURCE	SOURCE	IDENTIFIER
Experimental Models: Cell Lines		
HEK293	ATCC	CRL-1573; CVCL_0045
Oligonucleotides		
See Table S4 for list of TRPM2 mutants primers	This paper	N/A
Primer for hNUDT9H Forward: GGAATTCGACAGCTACCA CGTGAATGC	This paper	N/A
Primer for hNUDT9H Reverse: ATGCGGCCGCTTATTACTTA TCGTCGTCATCCTTGTAATCGTAGTGAGCCCCGAACTCA	This paper	N/A
Primer for hNUDT9H- E1409Q Forward: CGGATCCTCCGGC AGCAGCACTGGCCGTCTTTT	This paper	N/A
Primer for hNUDT9H-E1409Q Reverse: AAAAGACGGCCAG TGCTGCTGCCGGAGGATCCG	This paper	N/A
Recombinant DNA		
pcDNA3.1-human TRPM2	The A.M.Scharenberg Lab	N/A
pcDNA3.1-CD38	This paper	N/A
pCMV3-CD157	This paper	N/A
pGEX-4T-1 vector	Colwill et al., 2006	#11715; Addgene_11715
pGEX-4T-1-hNUDT9H	This paper	N/A
pGEX-4T-1-hNUDT9H-G1389A	This paper	N/A
Software and Algorithms		
Docking-Glide	Schrodinger 2018-1	https://www.schrodinger.com/
Molecular dynamic simulation	AMBER 11	http://ambermd.org/
Data analysis	CytExpert	https://cytexpert.updatestar.com/en/technical
Data analysis	Flowjo	https://www.flowjo.com/
Data analysis	Graph Pad Prism 6	https://www.graphpad.com/

LEAD CONTACT AND MATERIALS AVAILABILITY

Further information and requests for resources and reagents should be directed to and will be fulfilled by the Lead Contact, Wei Yang (yangwei@zju.edu.cn).

EXPERIMENTAL MODEL AND SUBJECT DETAILS

HEK293 cells were used to transiently express wild-type and mutant channels. Cells were maintained in Dulbecco's modified Eagle's medium DMEM supplemented with 50 units/mL penicillin and 50 μg/mL streptomycin (GIBCO, USA) and 10% fetal bovine serum, and were cultured at 37°C under a humidified atmosphere containing 5% CO_2. HEK293 cells are originally female in origin and its transient transfections were performed with Lipofectamine 2000 Transfection Reagent (Invitrogen, USA) according to the manufacturer's protocol

METHOD DETAILS

High performance liquid chromatography (HPLC)

Commercial cADPR was purified with HPLC, which was conducted on a C18 reversed phase column (Vemusil XBP C18, 10 μm, 100 Å, 10 × 150 mm), eluting with a linear gradient of 0%–60% CH_3CN in triethylammonium acetate buffer within 30 min at a flow rate of 1 mL/min. The column temperature was 20°C. The UV detection wavelength was 254 nm.

NAD^+ metabolites quantification in the experiments of cADPR hydrolase activity was conducted with HPLC using a 6 × 150 mm column packed with of AG MP-1 resin (Bio-rad). The nucleotides were eluted with a gradient of Trifluoroacetic acid (TFA). The TFA gradient was increased gradually from 5 to 30 mM in the first 15 min to elute cADPR and kept in 30 mM for 5 min to elute ADPR. HPLC of NAD^+ metabolites in the experiments of cADPR hydrolase incubation was also conducted on the same column, and products were eluted with a gradient of TFA from 0 to 67.5 mM over 22.5 min at a flow rate of 1 mL/min. The column temperature was 20°C. The UV detection wavelength was 260 nm.

Electrophysiology

Whole-cell current recordings were performed by using an Axopatch 200B amplifier (Molecular Devices) at room temperature or 37°C as described previously (Yu et al., 2017). Specifically, the extracellular solution contained 147 mM NaCl, 2 mM KCl, 1 mM $MgCl_2$, 2 mM $CaCl_2$, 10 mM HEPES, and 13 mM glucose, pH 7.4. The intracellular solution contained 147 mM NaCl, 0.05 mM EGTA, 1 mM $MgCl_2$, 10 mM HEPES, and cADPR at indicated concentrations, pH 7.3. The membrane potential was held at 0 mV, and a voltage ramp of 500 ms duration from −100 mV to 100 mV was applied every 5 s. Glass pipettes with a resistance of 3–5 MΩ were used. Data were acquired at 10 kHz and filtered offline during data analysis. Change of the extracellular solution was performed using a RSC-160 system (Bio-Logic Science Instruments).

Single channel recordings were performed using a HEKA EPC10 amplifier controlled with PatchMaster software (HEKA). The membrane potential was held at −80 mV and currents were elicited by gap-free protocol. The extracellular solution contained 145 mM NaCl, 5.6 mM KCl, 2 mM $MgCl_2$, 1.2 mM $CaCl_2$, and 10 mM HEPES, pH 7.3. The intracellular solution contained 140mM potassium gluconate, 4 mM NaCl, 2 mM $MgCl_2$, 10 μM $CaCl_2$, 1 mM EGTA, 10 mM HEPES, and 500 μM cADPR or 50 μM ADPR, pH 7.2. Data were filtered at 2.25 kHz and sampled at 12.5 kHz. Change of the extracellular solution was performed using a RSC-200 system (Bio-Logic Science Instruments). Single-channel data was processed by the QuB software version 1.4. Opening and closing events were detected during idealization with the half amplitude method.

NUDT9-H protein purification

The NUDT9-H domain of human TRPM2 protein (Uniprot O94759) containing a N-terminal glutathione (GST) tag followed by a thrombin cleavage site was constructed into pGEX-4T-1 vector and heterologously expressed in *E. coli* strain Rosetta (TransGen Biotech). Cells were cultured in LB media at 37°C until OD600 reached 0.6, followed by addition of isopropylthio-β-D-galactoside (IPTG) (Invitrogen) to give a final concentration of 0.2 mM. Cells were collected by centrifugation after further incubation for 24 h at 23°C, and cell pellets were resuspended at a concentration of 5-6 mL/g wet weight in Tris-EDTA buffer (20 mM Tris pH 7.4, 0.5 mM EDTA) supplemented with a protease inhibitor cocktail (containing 2 μg/mL DNase I, 0.5 μg/mL pepstatin, 2 μg/mL leupeptin and 1 μg/mL aprotinin, and 0.1 mM PMSF) and 0.5% N-dodecyl-β-d-maltopyranoside (DDM, Anatrace) and homogenized by sonication on ice. Then, the supernatant was collected by centrifugation at 14,000 *g* for 45 min and incubated with gluthathione Sepharose 4B resin (GE Healthcare) with gentle rotation at 4°C. After 3 h, the resin was collected on a disposable gravity column, incubated for 10 min with 5 bed volume wash buffer (20 mM Tris pH 7.4, 0.5 mM EDTA, 0.025% DDM). The GST-NUDT9-H was eluted with elution buffer containing 15 mM reduced gluthathione (BBI). 4 mg GST-NUDT9-H was then incubated with 2 U thrombin (GIBCO) with gentle rotation at 4°C for 24 h. The mixture was incubated with gluthathione Sepharose 4B resin again for 3 h. After collecting the resin on a disposable gravity column, the purified NUDT9-H (with no GST tag) in the flow through was collected. NUDT9-H were concentrated to over 1 mg/mL using a 10 kDa cut-off concentrator (Vivaspin2 GE Healthcare, 2 mL) and further purified by size exclusion chromatography on a Superdex 200 10/300 GL column (GE Heathcare) which was pre-equilibrated with wash buffer (20 mM Tris pH 7.4, 0.5 mM EDTA, 0.025% DDM).

Surface plasmon resonance

Binding affinities of cADPR, ADPR and NAD^+ to the NUDT9-H domain of human TRPM2 was determined on a Biacore T200 instrument (BIACORE T200, GE, USA). The NUDT9-H protein was immobilized on CM5 sensor chips by an amine-coupling procedure on flow cells channel 2–4, whereas flow cell 1 served as a negative control. Hundred microliters of a 1:1 mixture of 0.4 M 1-ethyl-3-(3-dimethyla-minopropyl carbodiimide (EDC) in H_2O and 0.1 M N-hydroxysuccinimide (NHS) in H_2O were injected at a flow of 30 μL/min for 420 s in order to activate the carbonyl group. The NUDT9-H protein was dissolved in sodium acetate acid buffer (pH 4.5) at a final concentration of 40 ug/mL with the injection time of 60 s, dissociation time of 60 s, flow rate 30 μL/min. Then, the sample was blocked with ethanolamine (1 M) in the other unbound regions of the sensor chip with a flow rate of 5 μL/min for 420 s to the final 8000 response units (RU). Sensor chips were primed twice with degassed physiological running buffer (0.02 M phosphate buffer saline (PBS), 2.7 mM KCl, 137 mM NaCl, 0.05% Surfactant P20, pH 7.4) and equilibrated at 50 mL/min until the baseline appeared stable. cADPR, ADPR and NAD^+ were dissolved in PBS with PPG-20 methyl glucose ether buffer (PBSP: 0.02 M PBS, 2.7 mM KCl, 137 mM NaCl, 0.05% Surfactant P20, pH 7.4), diluted to a concentration series, and injected starting from the lowest concentration. In all experiments, the analysis was performed at 25°C, defining an association time of 60 s and a dissociation time of 120 s at a flow of 30 μL /min. For calculating related k_a, k_d, and K_D values,the Biacore T200 evaluation software 2.0 (GE Healthcare) was used and 0 μM was used for fitting the curve by a Langmuir 1:1 stoichiometric algorithm.

cADPR hydrolase activity of HEK293 lysate

The assay was conducted as previously described (Fang et al., 2018). Briefly, HEK293 cells and the CD38-overexpressing (CD38 OE) HEK293 cells were lysed with lysis buffer (50 mM Tris, 150 mM NaCl, 1 mM EDTA, 0.5% Triton X-100, pH 7.4, protease inhibitors cocktail (Roche)). The endogenous nucleotides in the lysate were removed by dilution with centricon (Millipore, #MA54455). 150 μg total proteins were incubated with 0.4 mM cADPR in 100 μL of PBS for different time assays (0, 0.5, 1, 2 h). The reactants were diluted in 1 mL of 5 mM trifluoroacetic acid (TFA) and applied to HPLC analysis (see HPLC part).

Immunostaining and flow cytometry

HEK293 cells were maintained in Dulbecco's Modified Eagle Medium (DMEM) containing 10% fetal bovine serum (FBS) supplemented with 1% penicillin-streptomycin. 5×10^5 cells were transfected with 2 μg pcDNA3.1-CD38 or pCMV3-CD157 using Lipofectamine 2000 (Invitrogen) according to the manufacturer's instructions. After 48 h post-transfection, cells were detached by brief incubation with low concentration of trypsin (0.01%), which was safe for CD38 and CD157 proteins. 8×10^5 detached cells were rinsed with PBS, fixed in 2% paraformaldehyde (PFA) at 4°C for 15 min, washed and applied to staining process. For CD38 staining, cells were incubated in 1 μg/ml fluorescein isothiocyanate-labeled anti-CD38 (IB4)/BSA/PBS at room temperature for 30 min, washed with PBS and analyzed with a CytoFLEX flow cytometer (Beckman Coulter). For CD157 staining, cells were incubated in 0.5 μg/ml anti-CD157 at room temperature for 30 min, washed, incubated with fluorescent-labeled secondary antibody at room temperature for 30 min and analyzed by flow cytometry.

Docking and MD simulation

Docking study and MD simulation were conducted as previously described (Yu et al., 2017). In brief, the induced-fit docking (IFD) protocol in Glide was used (Friesner et al., 2004). The receptor-ligand complexes were found in the preliminary docking step and energy minimized to an induced-fit conformation. Then, induced docking was performed for cADPR within the NUDT9-H domain of human TRPM2 with an 18 × 18 × 18–Å cube. The structure of cADPR interacting with the NUDT9-H domain produced by the IFD procedure was further explored with MD simulations, by using the AMBER 11 software suite (University of California, San Francisco, San Francisco, CA). The general AMBER force field (gaff) and the ff99SB force field were used for the protein and ligand, respectively. A 15-ns data production run was performed. The absolute binding free energy (ΔG binding) was then predicted by applying the MM/GBSA approaches, using a total of 50 snapshots from 13–15 ns which were evenly extracted from the single MD trajectory. To illustrate the interactions between each residue and cADPR, we performed MM/GBSA decomposition analysis, all snapshots mentioned above were used.

cADPR hydrolase incubation

1 μg/mL reCD38 was added into 100 μM cADPR dissolved in 50 μL ICS (147 mM NaCl, 0.05 mM EGTA, 1 mM MgCl2, 10 mM HEPES, pH 7.3) and incubated at room temperature. The concentrations of cADPR and ADPR were determined using HPLC before and after incubation (see HPLC part).

QUANTIFICATION AND STATISTICAL ANALYSIS

Prism 6 software (GraphPad Software) was used for all statistical analyses. Electrophysiological recordings from at least four cells or independent parallel experiments were averaged and are presented in the text and figures as means ± SEM. Currents of the mutants were normalized with the mean maximal currents in cells expressing the WT TRPM2 channels recorded on the same day, which were referred to as the relative currents. Student's t test was applied to determine the significance of differences, except as otherwise indicated. Mann-Whitney U test was carried out to determine the significance of differences on channel open probability in the single channel recordings. $p < 0.05$ was considered to be statistically significant.